Materials & Design 255 (2025) 114183

Contents lists available at ScienceDirect

Materials & Design

journal homepage: www.elsevier.com/locate/matdes

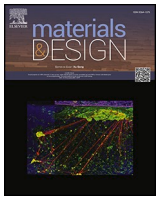

An experimental study of the moisture-induced degradation characteristics of GFRP-concrete interface

Jia-Xiang Liew [a], Peng Zhang [b], Ming-Feng Kai [c,*], Jian-Guo Dai [b,*]

[a] Department of Civil and Environmental Engineering, The Hong Kong Polytechnic University, Kowloon, Hong Kong, PR China
[b] Department of Architecture and Civil Engineering, City University of Hong Kong, Hong Kong 999077, China
[c] School of Mechanics and Construction Engineering, Jinan University, Guangzhou 510632, China

ARTICLE INFO

Keywords:
Interfacial degradation
Moisture exposure
Mirco-mechanics
Hydrolysis reaction
Fibre dissolution

ABSTRACT

The durability of FRP-concrete interfaces is critical for the long-term performance of FRP −reinforced concrete structures. However, the degradation mechanisms of this interface, particularly in moist environments, remain poorly understood. This study employs novel experimental methods to investigate the effects of moisture at the Glass FRP (GFRP)-concrete interface by analysing relative humidity, micro-mechanics and chemical properties using capacitive humidity sensors, nano-indentation, FTIR spectroscopy, SEM and EDS. The results demonstrate varying degradation levels across the glass fibre, interphase region and resin matrix, with the interphase region exhibiting the most rapid degradation. FTIR analysis revealed significant resin matrix hydrolysis due to the substantial breakage of vinyl ester chains. SEM and EDS analysis verified the dissolution process of glass fibres, as evidenced by their pitted surface morphology. The dissolution was predominantly localized to the fibres at the GFRP bar's surface, with the internal fibres maintaining their surface integrity. These findings provide critical insights into the moisture-induced degradation mechanisms at the GFRP-concrete interface, advancing the understanding of long-term durability in FRP-reinforced structures.

1. Introduction

Fibre-Reinforced Polymer (FRP) reinforcement, is an innovative construction material that is rapidly gaining popularity as an alternative to traditional steel reinforcement. Composed of high-strength fibres (e.g. glass, carbon, or aramid) embedded in a polymer matrix, FRP bars offer exceptional corrosion resistance, tensile strength and lightweight properties, making them well-suited for modern infrastructure applications [1]. As the construction industry shifts toward sustainable and low-maintenance solutions, FRP bars have emerged as a compelling choice, offering the potential to revolutionize the way we approach reinforced concrete [2].

Despite their corrosion resistance, FRP reinforcements are prone to chronic degradation in concrete environments, particularly under-moisture and alkaline exposure. Fergani et al. [3] discovered silicon, aluminium and calcium elements near degraded glass fibres in GFRP bars exposed to alkaline solutions, suggesting chemical reactions at the fibre–matrix interface. Ruiz Emparanza et al. [4] reported a 45 % reduction in tensile strength for seawater-immersed GFRP bars, followed by a 20 % decrease in transverse shear and bond strength, and a 10 % loss in horizontal shear strength. Similarly, Yu et al. [5] reported a deterioration of GFRP bars exposed to alkaline solutions, attributed to interfacial debonding between glass fibres and resin matrix, which led to a more pronounced reduction in interlaminar shear strength. However, the effects of moisture and cementitious material environment on the degradation of glass fibre and vinyl ester resin remains unclear with several contradictory findings for GFRPs. Elgabbas et al. [6] documented a 70.4 % strength retention ratio after 1440 h of alkali exposure, while Won et al. [7] reported 95.2 %, highlighting inconsistencies in current understanding.

These discrepancies could be attributed to the difficulties in characterizing moisture at the GFRP-concrete interface in relation to the changes in micro-mechanics and chemical evolution. Unlike external environments, moisture dissipates slowly in concrete, with internal relative humidity reaching 80 % in 50 mm thick samples after 4 weeks of water exposure [8,9]. In FRP-reinforced concrete, concrete serves as the surrounding environment of FRP bars, whose pore humidity, together with pore composition, plays a dominant role in the degradation of FRP bars but the influence of these relationships remains unresolved. The resin can absorb 1 % to 7 % moisture by weight, which plasticizes the

* Corresponding authors.
E-mail addresses: mfkai@jnu.edu.cn (M.-F. Kai), jiangdai@cityu.edu.hk (J.-G. Dai).

https://doi.org/10.1016/j.matdes.2025.114183
Received 6 February 2025; Received in revised form 28 May 2025; Accepted 1 June 2025
Available online 2 June 2025

matrix and induces differential swelling stresses while altering the physical properties [10,11]. This can further promote microcracks within the fibre-resin interface as a result of the breakage of polymer chains by hydrolysis [12]. On the other hand, SiO_2 present in glass fibres can hydrate with hydroxide ion (OH^-) and weaken the Si-O-Si bond [13]. To predict the absolute water content and pore saturation in cement-based materials, Strangfeld & Kruschwitz integrated internal relative measurements obtained from thermoset polymer capacitive sensors with Hillerborg theory [14]. This method was further developed to determine the diffusion coefficient and hydraulic conductivity of cement and calcium sulphate-based materials with varying thicknesses [15]. However, monitoring relative humidity at the GFRP-concrete interface still faces technical bottlenecks. At relative humidity above 90 %, the accuracy and uncertainty of measurements greatly intensifies. Moreover, obtaining relative humidity measurements at the FRP-concrete interface requires proper embedment methods without affecting the microstructure and cement chemistry surrounding the FRP bars. Attaining inspiration from techniques developed to monitor strain distribution and bond behaviour at the steel–concrete interface by bisecting reinforcing bars along their axis [16–21]. Relative humidity sensors can potentially be embedded within GFRP bars for monitoring and obtaining measurements from realistic conditions.

This study aims to investigate the moisture-induced degradation of GFRP-concrete interfaces, providing insight into the relative humidity, micro-mechanics and chemical evolution. Sand-coated GFRP bars were embedded in concrete with different water-to-cement ratios and exposed to different humidity environments (36 % and 86 %) for 2 – 4 months. Relative humidity changes at the GFRP-concrete interface were monitored by capacitive sensors, considering the interface is a critical location that reflects how the concrete environment influences the degradation of FRP bars. Surface morphology and chemical properties were examined with SEM and EDS, and the micro-mechanics were obtained from nanoindentation to explain the time-dependent degradation.

2. Sample preparation and test method

2.1. Materials

Concrete samples were prepared by mixing ordinary Portland cement with sand, gravel, and water, and the mixture design is shown in Table 1. Portland cement with strength class 52.5 N from Green Island Cement Co., Ltd. was used as the binder, and its physical properties and chemical composition are given in Table 2. Concrete mixtures with distinct pore structures were prepared using water-to-cement ratios of 0.35 and 0.5. The total aggregate proportion was fixed at 70 % and the properties of the river sand and gravel are provided in Table 3. Before casting, GFRP bars with a diameter of 10 mm were placed in 40 mm × 40 mm × 40 mm plastic moulds and held in place with adhesive to provide a 25 mm cover. The GFRP bars used were manufactured by Dextra Building Products (Guangdong) Co., Ltd using the pultrusion process with a volume fibre content of 81.2 %, elasticity modulus of 55.8 and ultimate strain of 1.87 [22,23]. Furthermore, a small diameter (10 mm) of GFRP bars was chosen for this study due to its convenience in preparing the GFRP-concrete samples and the following tests. Fresh concrete was mixed in a paddle mixer and cast into the moulds. Each mould was covered with a plastic film to avoid water evaporation to prevent dry shrinkage. After 24 h of curing, samples were demoulded and cured in moist conditions (95 %± 5 % RH; 21 °C± 2 °C) for 28 days. Subsequently, samples were conditioned in an incubator (21 °C± 2 °C) for two, three and four months until the mass loss became under 0.01 %. The incubator contained saturated magnesium chloride and potassium chloride salt solutions to control the environmental RH at 36 % and 86 %, respectively.

2.2. Sensor calibration and embedment

Key sensing and design specifications were reviewed before selecting the optimal relative humidity sensor for this study. Given the objective of embedding sensors within GFRP bars, a wireless solution was deemed unsuitable due to the dimensions of electronic circuit boards (exceeding 40 × 40 × 40 mm). Additionally, for laboratory-based research, the sensor must exhibit a response time of under 60 s to capture rapid humidity fluctuations, along with a sensing range of 10–90 % to effectively monitor GFRP degradation.

Following a thorough evaluation of available sensor technologies, DHT22 manufactured by Kuongshun Electronic was chosen for this study. The sensor employs a moisture-sensitive substrate that absorbs moisture from the environment which varies the electrical resistance to determine the humidity level. According to the manufacturer, the sensor achieves ± 2 % RH accuracy with a 0.1 RH resolution. The device is encased in a 12 × 16 × 7.7 mm package and designed to operate in temperatures ranging from −40 – 125 °C. To embed sensors in GFRP bars and reduce the amount of dead space, a 3D printed enclosure with the inner and outer diameters of 18 and 20 mm was designed on SolidWorks and exported to Ultimaker S5 Pro for printing shown in Fig. 1**c.** Subsequently, a 20 mm diameter hole was drilled into a 40 mm diameter sand coated GFRP bar with a 20 mm diameter drill bit. Before casting, the sensor was placed into the 3D-printed enclosure and sealed with silicone. This embedment method was chosen to minimize the potential local microstructural defects at the GFRP-concrete interface. GFRP bars were placed vertically and held in place with adhesive in plastic moulds to provide a 25 mm cover and prevent blockage of the cavity prior to compaction on a vibrating table.

The accuracy and response time of each sensor were evaluated in a temperature-controlled laboratory (21 ± 2 °C) prior to calibration (Fig. 1**a)**. A total of 15 individual sensors were tested in incubators containing saturated magnesium chloride (38 % RH) and sodium chloride (75 % RH) salt solutions. Each incubator was preconditioned with fresh salts for one week at 21 ± 2 °C, while relative humidity was monitored using an RS pro hygrometer. The calibration process consisted of placing sensors in incubators for 5 min intervals with readings recorded every 5 s. The acquired measurements were averaged and adjusted to the target RH values by modifying the Arduino's C++ code. Post-calibration results demonstrated significant improvement, reducing the maximum deviation from ± 10 % RH to ± 3 % RH (Fig. 2). According to the degradation model of GFRP bars [24], ±3% RH error indicated that the evolution of GFRP bars under concrete environment can be accurately predicted.

2.3. Finite element modelling (FEM)

FEM was performed to simulate the oven-drying process of the specimen, following the geometry specification and procedures detailed in Section 2.1. The simulation was performed using the commercial software COMSOL, incorporating a simple moisture transport model

Table 1
Mix proportions.

Mix design	w/c ratio	Water (kg/m^3)	Sand (kg/m^3) <5mm	Coarse aggregate (kg/m^3) <10 mm	Cement (kg/m^3)	Aggregate vol fraction: %
C-0.35-PC-70	0.35	156.1	729.9	1094.9	446	70
C-0.5-PC-70	0.5	182.4	729.9	1094.9	365	70

Table 2
Physical properties and chemical characteristics of cement used.

Index	Density (kg/m^3)	Fineness (kg/m^3)	Compressive strength (MPa)	Flexural strength (MPa)	Loss-on-ignition (%)	K_2O (%)	Na_2O (%)
Value	3100	3630	65.5	9.0	2.5	0.47	0.16

Table 3
Aggregate properties.

Aggregate type	MSA: mm	Density (kg/m^3)	Moisture absorption: %
Fine	5	2611	1.0
Coarse	10	2601	0.8

proposed by Sun et al. [25]. In this model, the primary variable is the degree of saturation (θ), governed by the following equation:

$$\frac{\partial\theta}{\partial t} = \nabla\cdot[D(\theta)\cdot\nabla\theta]$$

where $D(\theta)$ represents the effective moisture transport coefficient, defined as a function of capillary pressure p_c and vapour density ρ_v by:

$$D(\theta) = -\frac{1}{\rho_l\phi}\left(D_v\frac{M_w\rho_v}{\rho_l RT} + K_l\right)\frac{\partial p_c}{\partial\theta}$$

The equation uses, ρ_l for liquid water density; D_v for vapour diffusion coefficient, and K_l for liquid water permeability coefficient in concrete. M_w is the molar mass of water molecules; R is the universal gas constant; and T is the temperature. Capillary pressure p_c relates to degree of saturation θ via the water-vapour sorption isotherm (WVSI). This study utilizes the WVSI model established by Sun et al. [19]:

$$\begin{cases} \theta_w = 1 - \exp\left(\dfrac{2B\gamma\cos\alpha}{p_c}\right) \\ \theta_d = \left[1 - \exp\left(\dfrac{2B\gamma\cos\alpha}{p_c}\right)\right]\left\{1 - \ln\left[1 - \exp\left(\dfrac{2B\gamma\cos\alpha}{p_c}\right)\right]\right\} \end{cases}$$

where θ_w and θ_d represent the saturation levels during wetting and drying process respectively. The parameter B characterizes pore size distribution, γ represents surface tension of liquid water; and α indicates the contact angle between water and pore surfaces. Once the degree of saturation is determined, capillary pressure p_c can be calculated using Eq. (3), from which relative humidity (RH) can be determined from:

$$h = \exp\left(\frac{p_c M_w}{\rho_l RT}\right)$$

2.4. Experimental characterizations

2.4.1. Mechanical properties

In this study, a nano-indenter (Hysitron TI Premier, Bruker) equipped with Scanning Probe Microscopy (SPM) was employed to evaluate the indentation modulus and hardness of moisture-exposed FRP bars embedded in concrete (Fig. 3**a**). Upon reaching the target conditioning age (2, 3 and 4 months), sand-coated GFRP bars were extracted by applying a 10 kN compression load at a rate of 0.6 MPa/second (Fig. 3**b**). The retrieved bars were dry-cut using a diamond saw to produce disc-shaped specimens with a dimension of 10 mm and a height of 10 mm, which were then epoxy-impregnated in cylindrical moulds. After curing at 22 °C for 24 h, samples were demoulded and subjected to a multi-stage polishing process. Initial surface preparation involved removing a thin resin layer using 1200-grit SiC sanding paper, followed by sequential polishing with diamond suspensions (9 μm, 3 μm, and 0.05 μm) on appropriate polishing clothes, with each step lasting at least 10 min. Between polishing stages, samples were ultrasonically cleaned in ethanol to remove any residue particles. Finally, the surface roughness of samples was inspected on an area of 10 μm × 10 μm with a final root-mean-squared (RMS) roughness < 15 nm (Fig. 3**c**), ensuring adequate surface roughness for nanomechanical characterization of fibre-

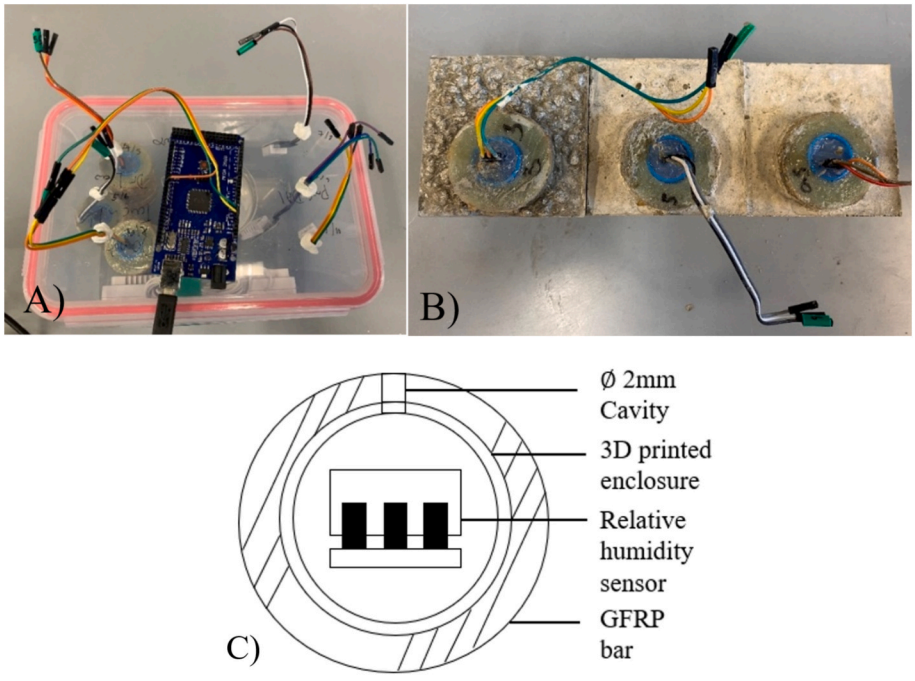

Fig. 1. Illustrations of the development of sensing method (a) calibration of sensors with saturated salts, (b) embedded sensors in concrete with 25 mm cover depth and (c) cross-section view of developed sensing method.

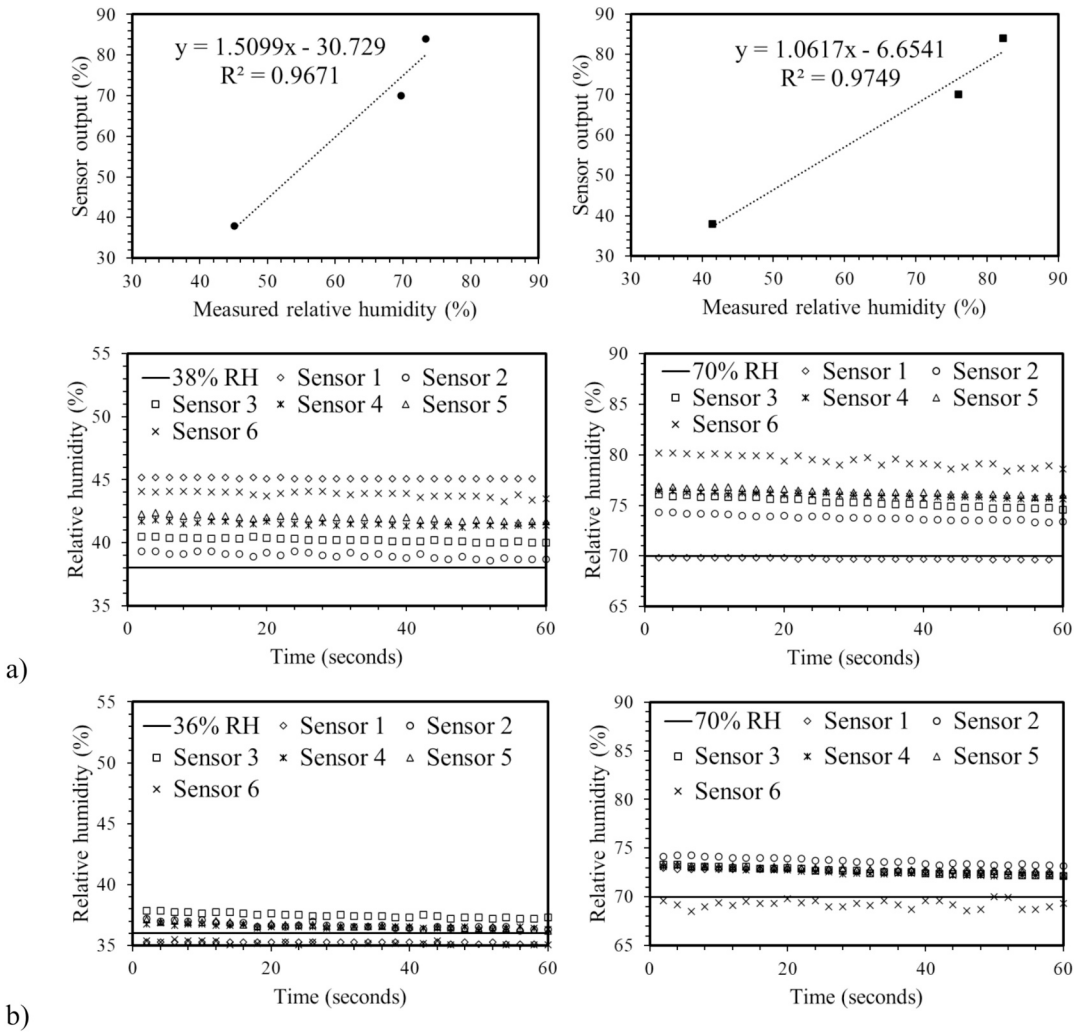

Fig. 2. Sensor measurements at varying relative humidity a) before and b) after calibration.

reinforced composite materials [26].

The nanoindentation tests employed a trapezoidal loading profile: 5 s loading to reach the maximum load of 3000 μN, 2 s holding at peak load, followed by 5 s unloading. Due to the relatively weak interfacial bonding between the vinyl ester matrix and glass fibres, the bulk composite has a more comparative ductile and soft mechanical behaviour. For each sample, eight distinct regions were analysed using a 4 × 4 indentation grid with 1 μm spacing, yielding 128 data points for robust statistical analysis (Fig. 3**d**). Error bars in Figs. 4 and 5 represent the measurement variability. Following each test, the reduced modulus (E_r) and hardness were directly obtained. The material elastic modulus (M) was then calculated by accounting for the indenter tip effects [27], using the following relationship:

$$M = \left(\frac{1}{E_r} - \frac{1-\nu_i^2}{E_i}\right)^{-1} \quad (1)$$

where E_i and ν_i are parameters of the indenter tip (E_i = 1140 Gpa and ν_i = 0.07 for a diamond tip).

2.4.2. Morphology and elemental composition analysis

The surface features of GFRP bars after nanoindentation were analysed using a TESCAN VEGA 3 scanning electron microscope equipped with energy-dispersive X-ray spectroscopy (SEM-EDS). The samples for SEM/EDS tests were prepared by splitting the GFRP bars directly to characterize the microstructure of GFRP bars. No cutting, grinding, polishing and washing were involved in the sample preparation. Next, a higher-resolution SEM was provided to examine the surface of GFRP samples. The surface of each sample was cleaned using ethanol followed by gold sputter coating. Subsequently, samples were mounted on microscopy stubs using conductive carbon tape. SEM examination was conducted at 20 kV accelerating voltage with approximately 10 mm working distance in high-resolution scan mode. EDS mapping was performed in the backscattered electron (BSE) mode at 3200 × magnification. The EDS data were collected based on 5 selected regions with each region tested for 10 times. Furthermore, the chemical structure of surface and internal GFRP bars was examined using Fourier transform infrared spectroscopy (FTIR) (Spectrum Two PerkinElmer, USA) with attenuated total reflectance (ATR) mode. Samples were prepared by obtaining a specimen at the surface of GFRP bars with a weight of approximately 2 mg, following the methods reported in previous studies [28]. A total of 64 scans were recorded with a spectral resolution of 1 cm^{-1}, covering the wavenumber range from 4000 to 400 cm^{-1}. Specifically, the spectral zones in the band between 3800 and 2900 cm^{-1} including the stretching mode of C=O (1736 cm^{-1}) and asymmetric stretch of carboxylate C-O (1581 cm^{-1}) were examined [29].

3. Results and Discussion

3.1. Micromechanical properties of GFRP

The indentation hardness of glass fibres at different depths (surface

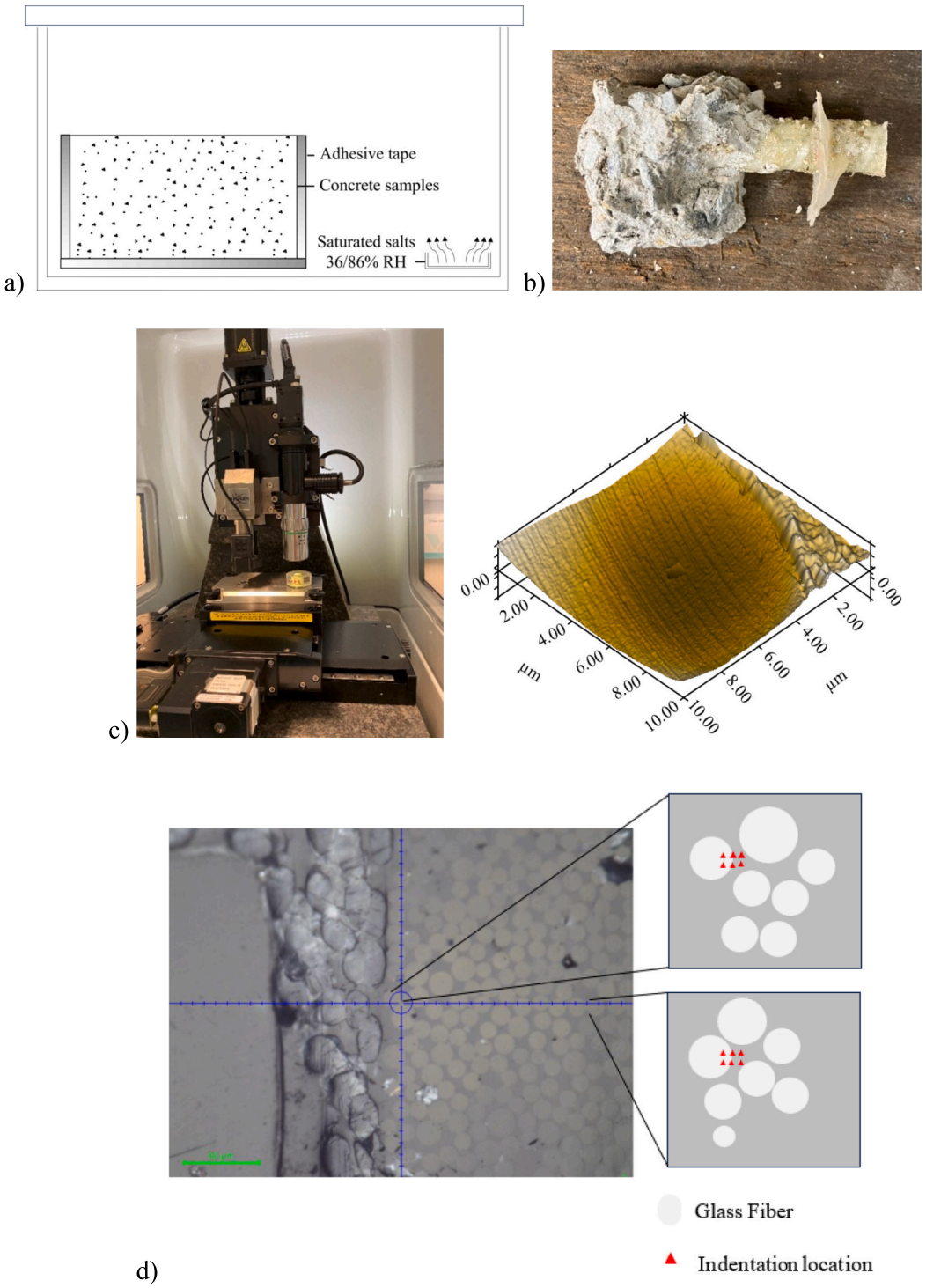

Fig. 3. Illustrations of methods applied to examine the mechanical properties of GFRP reinforcement bars (a) exposure to saturated salt solutions, (b) extraction of sample, (c) nano-indentation and (d) examining the hardness and reduced modulus of vinyl ester and glass.

and mid-section) was characterized, as shown in Fig. 4. On the GFRP surface (Fig. 4a), the hardness of glass fibres was initially 85 MPa, but decreased by 12.3 % (74 MPa) after exposure to 36 % RH for 3 months, proving an obvious degradation of glass fibres. At 86 % RH, the hardness dropped by 22.4 % after 3 months, showing a positive correlation between fibre degradation and environmental humidity. GFRP bars in concrete with a high w/c ratio experienced more significant degradation, likely due to the higher porosity caused by the high w/c ratio, which facilitated faster moisture diffusion. In contrast, within GFRP bars (Fig. 4b), the hardness values of glass fibres remained nearly identical, suggesting that deeply embedded fibres did not degrade significantly under high RH environments. Since the degradation occurred on the GFRP bar surface, the mechanical properties of the resin matrix and interphase region on the GFRP bar surface were further characterized (Fig. 5). The resin matrix exhibited a small-level hardness degradation, while the interphase region experienced 17.5 % and 27.5 % degradation after 3-month exposure to 36 % RH and 86 % RH, respectively. In summary, the degradation of GFRP bars occurs on the surface, with the

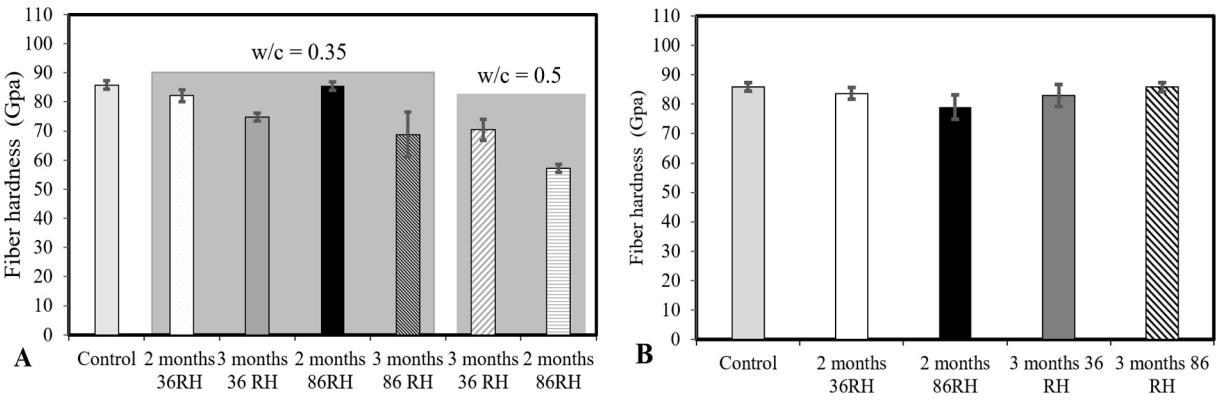

Fig. 4. Fibre hardness measured at A) GFRP surface and mid-section B) after different exposure conditions.

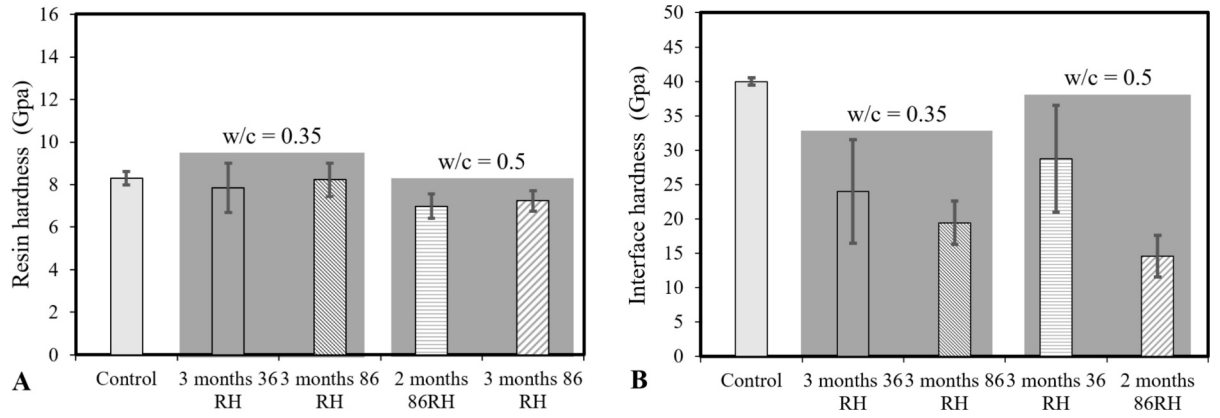

Fig. 5. Hardness of A) Resin and B) interface measured at the GFRP surface after different exposure conditions.

degradation rate following: interphase region > glass fibre > resin matrix.

3.2. Moisture characteristics

Fig. 6(a) and (b) present the experimental and simulated RH curves versus oven-dry time. The simulation closely aligns with experimental results, showing a 4 % difference for 0.35 w/c samples and a 1 % difference for 0.5 w/c samples, validating the FEM model accuracy and confirming negligible sensor embedding effects. Initially, the RH of concrete with a *w/c* ratio of 0.35 was lower than that with a *w/c* ratio of 0.5. After 200-hour drying, the RH of concrete with different *w/c* ratios almost reached an equilibrium, with a final RH value of ~ 30 %. Fig. 6(c) and (d) plot the evolution of sample weight and total moisture loss of GFRP-reinforced concrete during the drying process before exposure. For the samples with a *w/c* ratio of 0.35, the sample weight was reduced by 1.6 % with a total moisture loss of 12 g; while for those with a *w/c* of 0.5, the sample weight was reduced by 2.3 % with a total moisture loss of 16 g. These observations were expected because the water desorption of concrete is dependent on its capillary porosity. Samples with a lower *w/c* have a lower capillary desorption [30].

Fig. 7(a) and (b) present the experimental and simulated RH curves in relation to the exposure time at 86 % RH. The FEM simulation demonstrated excellent agreement with experimental data, showing a 3 % difference for 0.35 w/c samples and a 1 % difference for 0.5 w/c samples, respectively, confirming both model accuracy and negligible sensor embedding effects. The RH at the interface increased with the exposure time, with a lower *w/c* ratio samples exhibiting reduced RH due to its denser pore structure. Fig. 7(c) and (d) present the evolution of sample weight and total moisture gain of FRP-reinforced concrete during the exposure period (RH = 86 %). The evolution of sample weight was very limited, with a total moisture gain of 1.6 g and 1.7 g for the samples with *w/c* ratios of 0.35 and 0.5, respectively. It can be seen that the total moisture gain was significantly lesser, compared to the total moisture loss during drying (Fig. 6**d and e**). It should be noted that the evolution of sample weight, total moisture gain and RH of samples under 36 % RH exposure condition was not presented in this section because this exposure condition had a similar RH value to that (35 % RH) at the GFRP-concrete interface. Therefore, there is no evolution of sample weight and total moisture gain for concrete.

3.3. FTIR analysis

FTIR was utilized to examine the chemical changes in the polymeric chain of resin after exposure, aiming to study the effect of moisture on the chemical phases of resin. The peak frequency and spectrum of the FTIR spectrum are shown in Fig. 8. To provide more precise insights into the reaction kinetics, the peak deconvolution of the FTIR spectrum was analysed to quantitatively measure the intensity changes in the hydroxyl group (–OH) and the stretching bands of C=O and C-O bonds, as shown in Table 4. According to Fig. 8 and Table 4, a substantial reduction in C=O was observed with the increasing exposure time, suggesting significant breakage at the end (ester groups) of the vinyl ester chain in the resin matrix. Correspondingly, a rise in the C-O and O-H peaks was detected due to the formation of carboxyl (–COOH) groups. This phenomenon is so-called hydrolysis, and an increase in w/c ratio led to a higher degree of hydrolysis [31–34].

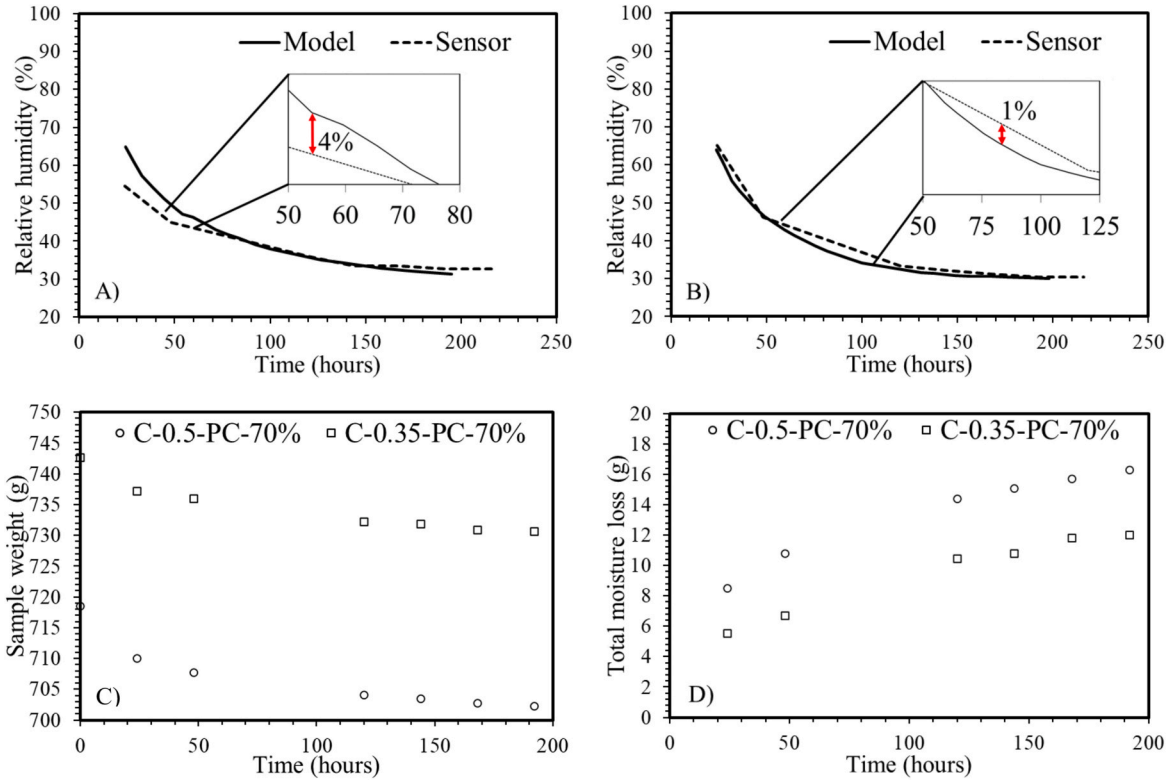

Fig. 6. The experimental and simulated RH curves for b) 0.35 w/c and c) 0.5 w/c samples dried in 40 °C oven, along with d) sample weight, and e) total moisture loss.

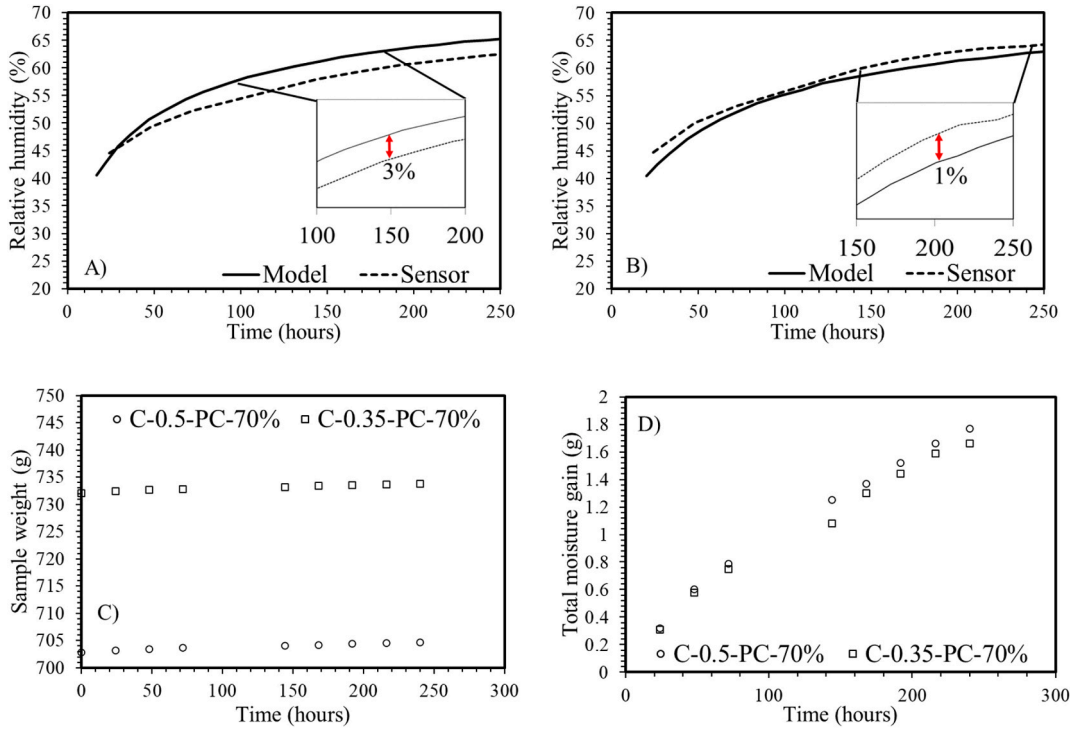

Fig. 7. The experimental and simulated RH curves for b) 0.35 w/c and c) 0.5 w/c samples conditioned at 86 % RH, along with d) sample weight, and e) total moisture gain.

3.4. SEM and EDS characterization

Fig. 9 presents representative images of the cross-section of GFRP bars to examine their overall microstructural changes at the surface and midsection under different exposure conditions. Overall, SEM analysis of cross-section images suggested no signs of microstructural

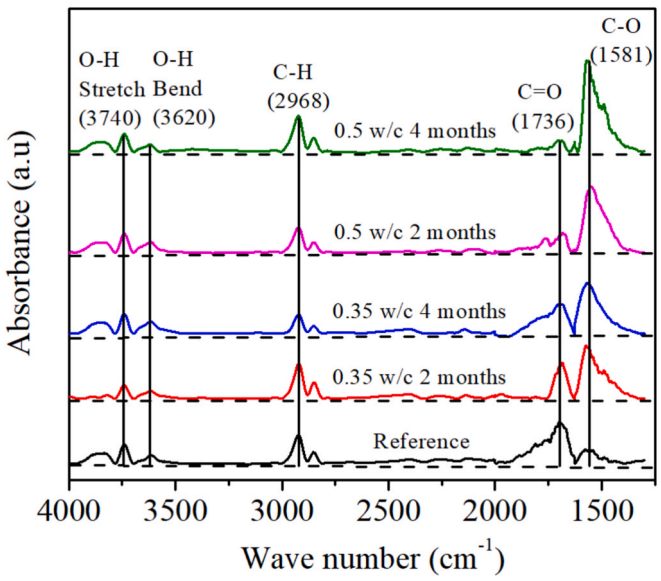

Fig. 8. FTIR analysis of resin conditioned at 86 RH.

Table 4
Spectrum result for FTIR analysis of resin conditioned at 86 RH.

Samples	OH/CH	C=O	C-O
Reference	**0.33**	**181.4**	43.90
w/c = 0.35			
2 months	0.43	70.00	190.30
4 months	1.36	29.14	192.00
w/c = 0.5			
2 months	0.63	37.28	235.90
4 months	1.44	28.50	278.10

deterioration at the GFRP bars. The increase in *w/c* ratio also did not cause the microstructural deterioration of the GFRP bars. Notably, voids and defects were discovered at the surface, which is mainly attributed to localized manufacturing defects [35–37].

Next, high-resolution SEM images were captured, scanning the surface and mid-section of the split GFRP bar samples, as shown in Fig. 10 (a). For the glass fibres on the GFRP bar's surface, some pits were observed on their surfaces, and the increasing w/c ratio led to more pits. These pits could be viewed as direct proof of the dissolution of glass fibres. However, the glass fibres in the mid-section of GFRP bars maintained their surface integrity, suggesting no dissolution of glass fibres in the internal GFRP bars. To further examine the chemical elements of glass fibres and resin at the surface and mid-section of GFRP bars, EDS analysis was performed, shown in Fig. 10(b). The EDS data were collected based on 5 selected regions with each region tested for 10 times. For the pitted surface of glass fibres, EDS focused on the pits to test their chemical elements. Compared to the intact surfaces in the mid-section, the pitted ones had a higher percentage weight of sodium (Na) and potassium (K), indicating the degradation of glass fibre at the pits. The percentage weight of these two elements increased with the w/c ratios, corresponding to a higher degree of dissolution of glass fibres. On the other hand, the silicon (Si) in the resin on the GFRP bar's surface increased, which was also evidence of the dissolution of glass fibres. These findings were similar to experimental work conducted by Zhao et al. [38].

4. Conclusions

This study systematically investigated moisture-induced degradation at the GFRP-concrete interface through an integrated approach combining capacitive humidity sensors, nanoindentation, SEM and EDS analysis. This provided insights into the relative humidity, micromechanics and chemical evolution. The key findings are summarized as follows:

(1) Moisture exposure caused distinct degradation patterns across the glass fibre, interphase region and resin matrix. The interphase

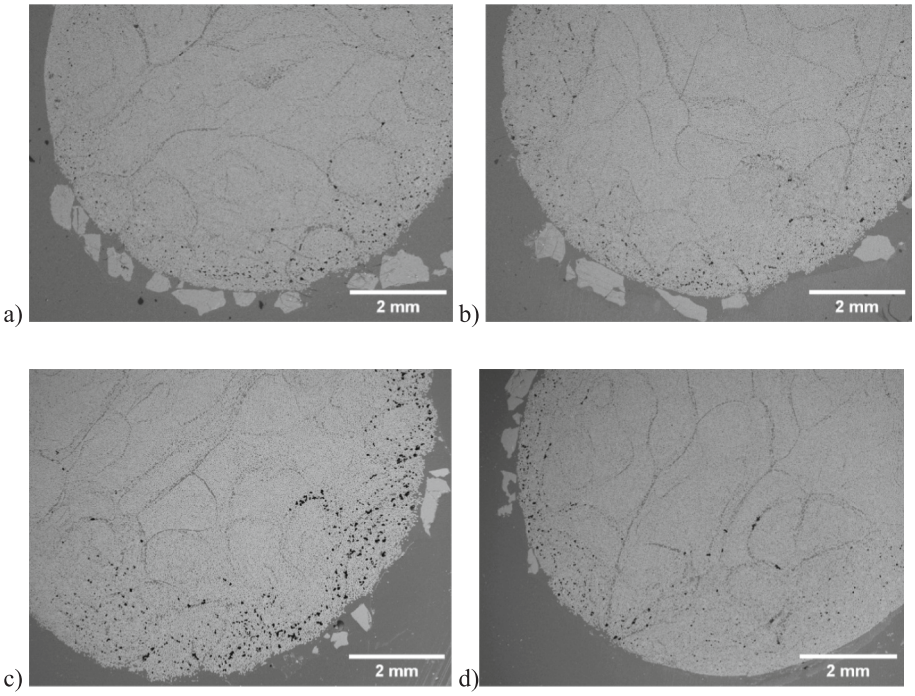

Fig. 9. SEM images of the microstructure of GFRP bars embedded in concrete condition at 86 RH for a) 3 months with 0.35 *w/c* ratio, b) 4 months with 0.35 *w/c* ratio, c) 3 months with 0.5 *w/c* ratio and d) 4 months with 0.5 *w/c* ratio.

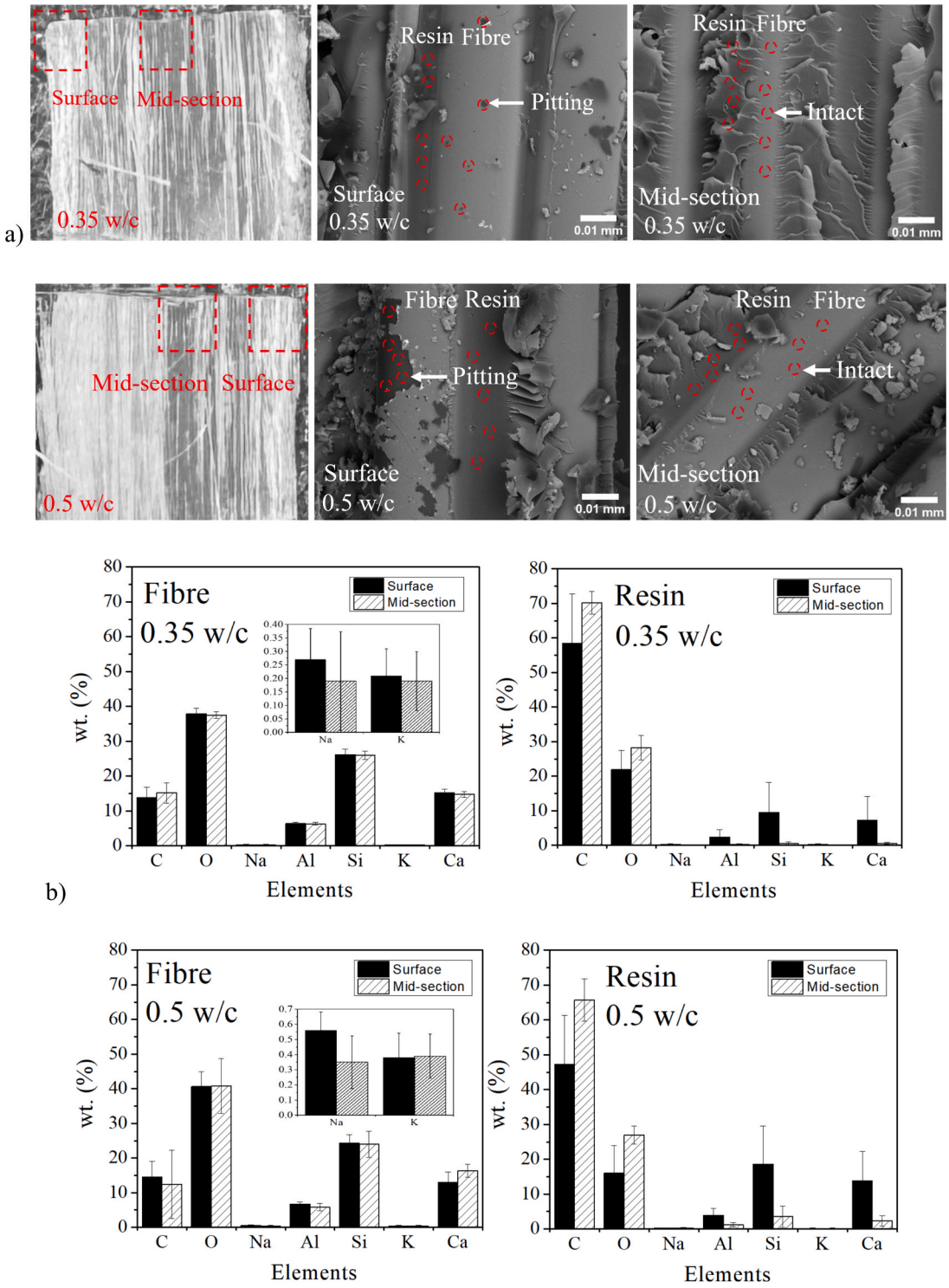

Fig. 10. A) high-resolution sem images of the surface and mid-section of the split gfrp bar samples after exposure to 86 rh for 4 months with b) EDS analysis.

region exhibited the most severe degradation, followed by the resin matrix and glass fibers. Higher *w/c* ratios accelerated degradation due to increased concrete porosity for moisture transport.

(2) The RH at the GFRP-concrete interface was accurately monitored by the humidity sensors. In an 86 % RH environment, the RH at the interface increased with the exposure time, and the sample with a lower *w/c* ratio had a lower RH after the exposure due to its denser pore structure. In a 36 % RH environment, the RH change at the interface was ignorable due to the balance between internal and external RH.

(3) FTIR analysis revealed that a significant hydrolysis reaction had occurred for the resin matrix due to the breakage of the end (ester groups) of the vinyl ester chain. This was evidenced by a noticeable increase in C-O and O-H peaks, corresponding to the formation of carboxyl (–COOH) groups. Additionally, an increase in w/c ratio led to a higher degree of hydrolysis for the resin matrix.

(4) High-resolution SEM images revealed that glass fibres on the surface of GFRP bars developed pits, with their severity increasing at higher w/c ratios. In contrast, fibres in the mid-section remained intact, confirming that degradation was primarily a surface phenomenon. EDS results further supported these observations, showing increased Na/K elements in the pitted regions and Si accumulation in the surrounding resin.

CRediT authorship contribution statement

Jia-Xiang Liew: Writing – original draft, Methodology, Investigation, Conceptualization. **Peng Zhang:** Writing – review & editing, Validation, Conceptualization. **Ming-Feng Kai:** Writing – review & editing, Conceptualization. **Jian-Guo Dai:** Writing – review & editing, Supervision, Investigation, Conceptualization.

Declaration of competing interest

The authors declare that they have no known competing financial interests or personal relationships that could have appeared to influence the work reported in this paper.

Acknowledgments

This research was supported by Guangdong Province R&D Plan for Key Areas (Project code: 2019B111107002), the Hong Kong Research Grants Council – Theme-based Research Scheme (Project code: T22-502/18-R), and The startup funding of the City University of Hong Kong "Advanced Functional Construction Materials (AFCM) for Sustainable Built Environment" (Project code 9380165).

Data availability

Data will be made available on request.

References

[1] B. Benmokrane and H. Rahman, in Proceedings of the First International Conference on Composite for Construction, 1998.
[2] K. Iwama, M.-F. Kai, J.-G. Dai, P. Zhang, P. Wang, C.-S. Poon, C.-K.-Y. Leung, K. Maekawa, Physicochemical-mechanical simulation of the short- and long-term performance of FRP reinforced concrete beams under marine environments, Eng Struct 308 (2024) 118051.
[3] H. Fergani, M. Di Benedetti, C. Miàs Oller, C. Lynsdale, M. Guadagnini, Durability and degradation mechanisms of GFRP reinforcement subjected to severe environments and sustained stress, Constr Build Mater 170 (2018) 637–648.
[4] A. Ruiz Emparanza, R. Kampmann, F. De Caso, C. Morales, A. Nanni, Durability assessment of GFRP rebars in marine environments, Constr Build Mater 329 (2022) 127028.
[5] Y. Yu, S. Liu, Y. Pan, X. Miu, J. Liu, Durability of glass fiber-reinforced polymer bars in water and simulated concrete pore solution, Constr Build Mater 299 (2021) 123995.
[6] F. Elgabbas, E.A. Ahmed, B. Benmokrane, Physical and mechanical characteristics of new basalt-FRP bars for reinforcing concrete structures, Constr Build Mater 95 (2015) 623–635.
[7] J.-P. Won, S.-J. Lee, Y.-J. Kim, C.-I. Jang, S.-W. Lee, The effect of exposure to alkaline solution and water on the strength–porosity relationship of GFRP rebar, Compos B Eng 39 (2008) 764–772.
[8] S.K. Padala, S. Bishnoi, B. Bhattacharjee, Long-term moisture penetration in concrete exposed to marine tidal conditions, Mag. Concr. Res. 74 (2022) 740–755.
[9] M. W. J., W. D. W. and C. T. M., Surface Zone Concrete: Drying, Absorption, and Moisture Distribution, Journal of Materials in Civil Engineering, 2001, 13, 49–57.
[10] C.L. Soles, F.T. Chang, B.A. Bolan, H.A. Hristov, D.W. Gidley, A.F. Yee, Contributions of the nanovoid structure to the moisture absorption properties of epoxy resins, J Polym Sci B Polym Phys 36 (1998) 3035–3048.
[11] W.-H. Liu, M.-F. Kai, P. Zhang, T. Yu, J.-G. Dai, Three-dimensional finite element modeling of debonding failure of skew FRP-bonded concrete joints, Eng Struct 303 (2024) 117537.
[12] H.P. Abeysinghe, W. Edwards, G. Pritchard, G.J. Swampillai, Degradation of crosslinked resins in water and electrolyte solutions, Polymer (guildf) 23 (1982) 1785–1790.
[13] Y.A. Al-Salloum, S. El-Gamal, T.H. Almusallam, S.H. Alsayed, M. Aqel, Effect of harsh environmental conditions on the tensile properties of GFRP bars, Compos B Eng 45 (2013) 835–844.
[14] C. Strangfeld, S. Kruschwitz, Monitoring of the absolute water content in porous materials based on embedded humidity sensors, Constr Build Mater 177 (2018) 511–521.
[15] C. Strangfeld, Determination of the diffusion coefficient and the hydraulic conductivity of porous media based on embedded humidity sensors, Constr Build Mater.
[16] R. M. Mains, in Journal proceedings, 1951, vol. 48, pp. 225–252.
[17] B. Bresler, V. Bertero, Behavior of reinforced concrete under repeated load, J. Struct. Div. 94 (1968) 1567–1590.
[18] F. Lagier, B. Massicotte, J.-P. Charron, Experimental investigation of bond stress distribution and bond strength in unconfined UHPFRC lap splices under direct tension, Cem Concr Compos 74 (2016) 26–38.
[19] J.-M. Henault, M. Quiertant, S. Delepine-Lesoille, J. Salin, G. Moreau, F. Taillade, K. Benzarti, Quantitative strain measurement and crack detection in RC structures using a truly distributed fiber optic sensing system, Constr Build Mater 37 (2012) 916–923.
[20] A. Barrias, J.R. Casas, S. Villalba, Embedded distributed optical fiber sensors in reinforced concrete structures—A case study, Sensors 18 (2018) 980.
[21] T. Galkovski, Y. Lemcherreq, J. Mata-Falcón, W. Kaufmann, Fundamental studies on the use of distributed fibre optical sensing on concrete and reinforcing bars, Sensors 21 (2021) 7643.
[22] J.-K. Zhou, Z.-H. Hao, J.-J. Zeng, S.-Z. Feng, Q.-J. Liang, B. Zhao, R. Feng, Y. Zhuge, Durability assessment of GFRP bars embedded in UHP-ECCs subjected to an accelerated aging environment with sustained loading, Constr Build Mater 419 (2024) 135364.
[23] L. Zhou, Y. Yu, Y. Zheng, Y. Ye, Y. Wang, J. Lao, Investigation on bond behavior of GFRP bar embedded in ultra-high performance polyoxymethylene fiber reinforced concrete, Eng Struct 324 (2025) 119324.
[24] P. Wang, Y. Zhou, Y. Lu, L. Ke, H. Wu, W. Li, C.K.Y. Leung, Predicting long-term tensile degradation of GFRP rebars embedded in concrete with a reconsidered environmental reduction factor CE, Dev. Built Environ. 20 (2024) 100583.
[25] C. Sun, L. Yuan, X. Zhai, F. Qu, Y. Li, B. Hou, Numerical and experimental study of moisture and chloride transport in unsaturated concrete, Constr Build Mater 189 (2018) 1067–1075.
[26] S.K. Khanna, R.M. Winter, P. Ranganathan, S.B. Yedla, M. Kalukanimuttam, K. Paruchuri, Sample preparation techniques for nano-mechanical characterization of glass fiber reinforced polyester matrix composites, Compos Part A Appl Sci Manuf 34 (2003) 53–65.
[27] M. Hardiman, T.J. Vaughan, C.T. McCarthy, Fibrous composite matrix characterisation using nanoindentation: the effect of fibre constraint and the evolution from bulk to in-situ matrix properties, Compos Part A Appl Sci Manuf 68 (2015) 296–303.
[28] W. Wu, X. He, W. Yang, L. Dai, Y. Wang, J. He, Long-time durability of GFRP bars in the alkaline concrete environment for eight years, Constr Build Mater 314 (2022) 125573.
[29] M. Robert, B. Benmokrane, Effect of aging on bond of GFRP bars embedded in concrete, Cem Concr Compos 32 (2010) 461–467.
[30] M.R. Nokken, R.D. Hooton, Dependence of rate of absorption on degree of saturation of concrete, Cement, Concrete and Aggregates 24 (2002) 20–24.
[31] H. El-Hassan, T. El-Maaddawy, A. Al-Sallamin, A. Al-Saidy, Performance evaluation and microstructural characterization of GFRP bars in seawater-contaminated concrete, Constr Build Mater 147 (2017) 66–78.
[32] H. El-Hassan, T. El-Maaddawy, A. Al-Sallamin, A. Al-Saidy, Durability of glass fiber-reinforced polymer bars conditioned in moist seawater-contaminated concrete under sustained load, Constr Build Mater 175 (2018) 1–13.
[33] Q. Xie, Q. Duan, G. Xia, J. Li, K. Yin, J. Xie, Effect of liquid diffusion and segregation on GFRP insulation performance in typical hygrothermal environment, Compos B Eng 244 (2022) 110152.
[34] P. Wang, L. Ke, H. Wu, C.K.Y. Leung, Effects of water-to-cement ratio on the performance of concrete and embedded GFRP reinforcement, Constr Build Mater 351 (2022) 128833.
[35] J.F. Davalos, Y. Chen, I. Ray, Long-term durability prediction models for GFRP bars in concrete environment, J Compos Mater 46 (2011) 1899–1914.
[36] G. Omid, N. Antonio, GFRP reinforcement in concrete after 15 Years of Service, J. Compos. Constr. 21 (2017) 04017024.
[37] S. Ramanathan, V. Benzecry, P. Suraneni, A. Nanni, Condition assessment of concrete and glass fiber reinforced polymer (GFRP) rebar after 18 years of service life, Case Stud. Constr. Mater. 14 (2021) e00494.
[38] Z. Qi, Z. Xiao-Ling, Z. Daxu, D. Jian-Guo, X. Xuanyi, Degradation of GFRP Bars with epoxy and vinyl Ester matrices in a Marine concrete environment: an Experimental study and theoretical modeling, J. Compos. Constr. 28 (2024) 04024004.